Ab initio phonon dispersions of wurtzite AlN, GaN, and InN

Claudia Bungaro,* Krzysztof Rapcewicz, and J. Bernholc
Department of Physics, North Carolina State University, Raleigh, North Carolina 27695-8202
(Received 27 September 1999)

Phonon excitations play an important role in electronic transport, nonradiative electron-relaxation processes, and other properties of interest for materials characterization, device engineering, and design. We have calculated the phonon dispersions and density of states for wurtzite AlN, GaN, and InN using state-of-the-art density-functional perturbation theory. The calculations are in good agreement with the existing experimental data for zone-center modes and predict the full phonon dispersions throughout the Brillouin zone. In particular, it is found that the three-phonon decay of the LO phonon in two acoustic phonons is not allowed in GaN and InN, since the LO frequency is much larger than the acoustic frequencies over the entire spectrum.

I. INTRODUCTION

The substantial potential of the group-III nitrides and their alloys for applications in optoelectronic and high speed devices has attracted a great deal of interest. AlN, GaN, and InN have direct energy gaps which span a substantial range, from the visible to the ultraviolet region of the spectrum. Consequently, their alloys have direct gaps that can be tuned to any value within this range simply by varying the alloy composition. This tunability offers many possibilities for device engineering. In particular, InGaN alloys were used in the realization of light emitting diodes and laser diodes operating in the blue and UV spectral region. Under ambient conditions, the III nitrides crystallize in a hexagonal, wurtzite (2H) structure, although thin films having a cubic, zinc-blende (3C) structure have also been grown.[1]

Properties of interest for device engineering and design, such as electronic transport, nonradiative electron relaxation processes, lattice specific heat, etc., are strongly influenced by phonon excitations. Furthermore, a number of nondestructive experimental techniques of sample characterization, for instance, Raman spectroscopy or IR reflectivity, involve phonon measurements. A characterization of the phonon dispersions and densities of states for the group-III nitrides is therefore desirable. However, since it is very challenging to grow single crystals of suitable size for neutron-scattering experiments, there are no experimental data for the phonon dispersions of these compounds. Only very recently have the phonon density of states for AlN and GaN been obtained from time-of-flight neutron spectroscopy using bulk powders.[2,3] In addition, numerous studies of the zone-center phonons in GaN and AlN films have been conducted using Raman and IR spectroscopy. Due to the lack of lattice-matched substrates, these samples are affected by the high density of defects and strain present in the films and it is therefore unclear how well these data represent the true bulk values. The least studied of the three nitrides is InN for which there are only few Raman studies.[4,5]

To the best of our knowledge, there have been no theoretical studies of the phonons of InN. For wurtzite GaN, *ab initio* calculations have been performed only for the zone-center phonons, while the full phonon spectrum has been calculated for the cubic zinc-blende structure.[6] Finally, the phonon-dispersion curves for AlN have been calculated for both the cubic and hexagonal crystal structures.[7]

As a result of the lack of experimental data, calculations based on empirical models, which depend on parameters fitted to experimental data, cannot give an accurate description of the lattice dynamics and the predictive power of *ab initio* calculations is needed. In this paper, we present an *ab initio* study of the phonon dispersions and the density of states for wurtzite AlN, GaN, and InN using state-of-the-art density-functional perturbation theory.[8,9] This method has been used for a large number of materials, including semiconductors, insulators and metals, and provides an excellent description of the vibrational properties with an accuracy better than a few percent of the calculated frequencies.

II. METHOD

The calculations have been performed using density-functional theory within the local-density approximation, separable norm-conserving pseudopotentials and a plane-wave basis-set with an energy cutoff of 65 Ry. The Perdew-Zunger parametrization of the exchange-correlation energy was used. Nonlocal, norm-conserving pseudopotentials[10–12] were applied with the Kleinman-Bylander approach.[13] Our Ga pseudopotential includes the nonlinear core correction (NLCC) and permits an accurate description of the GaN structural and dynamical properties without the need for an explicit treatment of the $3d$ electrons.[14,15] This is in agreement with another work on the lattice dynamics of GaN (Ref. 16) in which accurate results were obtained using the NLCC to treat the significant overlap of the $3d$ electrons with the valence states. To describe the In ions, we used a pseudopotential that includes the $4d$ electrons as valence states and was generated with the Troullier-Martins scheme.[17] We found that the explicit treatment of In $4d$ electrons is necessary for an accurate description of the lattice-dynamical properties.

To calculate the integrals over the Brillouin zone (BZ), the 12 special points of Chadi and Cohen[18] were chosen. We verified that the number of plane waves and the BZ sampling were sufficient to guarantee a convergence of 1 cm^{-1} for the calculated phonon frequencies.

We studied the lattice-dynamical properties using density-

TABLE I. Equilibrium lattice parameters a and c, c/a ratios, internal parameters u and bulk moduli B_0 for wurtzite AlN, GaN, and InN, compared with experimental data and other *ab initio* calculations.

		a (Å)	c (Å)	c/a	u	B_0 (Mbar)
AlN	This work	3.10	5.01	1.615	0.380	2.01
	Theory [a]	3.08	4.95	1.604	0.381	2.05
	Theory [b]	3.08	4.94	1.605	0.382	2.15
	Experiment [c]	3.11	4.98	1.601	0.382	2.02
GaN	This work (NLCC)	3.20	5.22	1.630	0.376	1.91
	Theory [d] (NLCC)	3.14	5.11	1.626	0.377	2.15
	Theory [a] (3*d*)	3.16	5.14	1.626	0.377	2.02
	Experiment [c]	3.19	5.20	1.630	0.377	1.95, 2.37
InN	This work (4*d*)	3.48	5.64	1.620	0.378	1.44
	This work (NLCC)	3.55	5.79	1.630	0.375	1.62
	Theory [a] (4*d*)	3.50	5.67	1.619	0.378	1.39
	Experiment [c]	3.54	5.71	1.613		1.26, 1.39

[a]Pseudopotential, Wright *et al.* Ref. 25.
[b]Pseudopotential, Karch *et al.* Ref. 7.
[c]Experimental data follow Ref. 25.
[d]Pseudopotential, Karch *et al.* Ref. 6.

functional perturbation theory (DFPT) with which the dynamical matrices at any $\mathbf{q}$ point in the BZ can be computed (see Ref. 9 for full details). The dynamical matrices were calculated on a uniform grid in the unit cell of the reciprocal space defined by $\mathbf{q}_{lmn}=(l/L)\mathbf{G}_1+(m/M)\mathbf{G}_2+(n/N)\mathbf{G}_3$, where $\mathbf{G}_1$, $\mathbf{G}_2$, and $\mathbf{G}_3$ are the reciprocal-space basis vectors and $0\leqslant l<L-1$, $0\leqslant m<M-1$, $0\leqslant n<N-1$. For a nonpolar material the dynamical matrix is analytic in reciprocal space and the interatomic force constants are short-range and negligible beyond a certain range $R_{\max}$. In this case, the interatomic force constants can be obtained with a Fourier transform of the dynamical matrix on a discrete mesh of spacing $\Delta q\leqslant 2\pi/R_{\max}$. The interatomic force constants so obtained can be used to compute the dynamical matrices at

TABLE II. The components of the Born effective charge tensor $\mathbf{Z}^*$ and the dielectric tensor $\boldsymbol{\epsilon}^{\infty}$, perpendicular ($\perp$) and parallel ($\parallel$) to the c axis, and their average values.

		$Z^*_{\perp}$	$Z^*_{\parallel}$	Z^*	$\epsilon^{\infty}_{\perp}$	$\epsilon^{\infty}_{\parallel}$	ϵ^{∞}
AlN	This work	2.70	2.85	2.75	5.17	5.36	5.23
	Theory [a]	2.53	2.69	2.58	4.38	4.61	4.46
	Theory [b]		2.67[d]		3.91	3.77	3.86
	Theory [c]		2.70[e]		4.42	4.70	4.51
	Experiment [f]			2.57			4.84[g]
	Experiment [h]						4.68
GaN	This work	2.69	2.86	2.75	6.11	6.38	6.20
	Theory [i]	2.60	2.74	2.65	5.21	5.41	5.28
	Theory [b]		2.74[d]		4.71	4.62	4.68
	Theory [c]		2.72[e]		5.54	5.60	5.56
	Experiment [l]	2.65	2.82	2.74			5.35
	Experiment [m]			3.2 ± 0.5			5.8 ± 0.4
InN	This work	2.78	2.96	2.84	7.61	7.96	7.73
	Theory [b]		3.02[e]		7.27	6.94	7.16
	Experiment [n]						8.4

[a]Pseudopotential, Karch *et al.* Ref. 7.
[b]LMTO, Christensen *et al.* Ref. 26.
[c]Pseudopotential, Chen *et al.* Ref. 27.
[d]Pseudopotential, Shimada *et al.* Ref. 28.
[e]Pseudopotential, Bernardini *et al.* Ref. 29.
[f]Raman data, Sanjurjo *et al.* Ref. 30.
[g]IR reflectivity, Collins *et al.* Ref. 31.
[h]IR reflectivity, Akasaki *et al.* Ref. 32.
[i]Pseudopotental, Karch *et al.* Ref. 6.
[j]Experimental data from Ref. 33.
[k]Experimental data from Ref. 34.
[l]From refractive index Ref. 35.

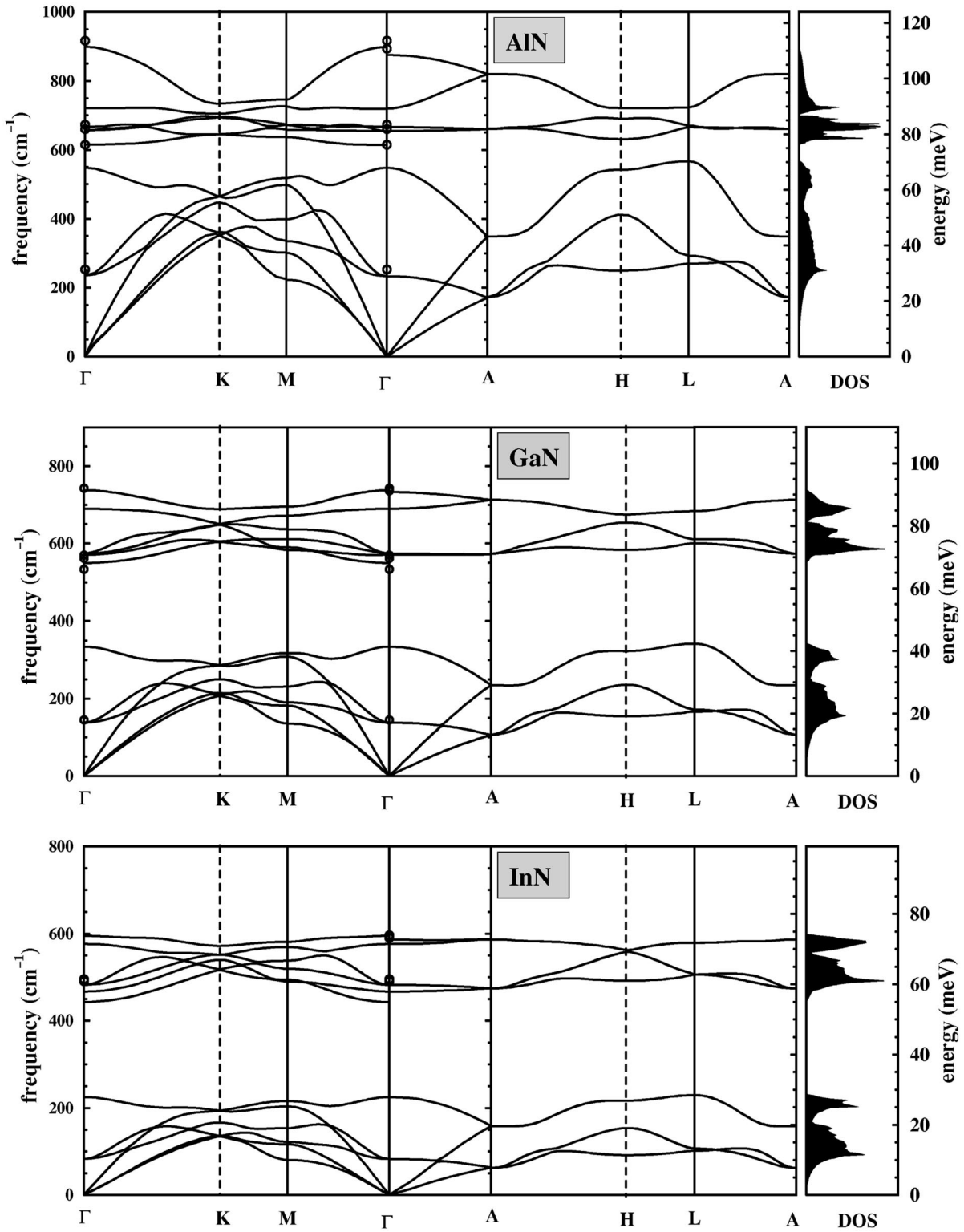

FIG. 1. *Ab initio* phonon dispersions and density of states (DOS) for AlN, GaN, and InN in the wurtzite structure. The scales of phonon frequencies in AlN, GaN, and InN are mainly determined by the masses of Al, Ga, and In, respectively. The discontinuity observed in the optical-phonon dispersion at Γ (most obvious in AlN) is due to the long-range nature of the Coulomb interaction in the polar III-nitrides, and to the anisotropy of the wurtzite structure. It is shown in more detail in Fig. 2. Circles: Raman-scattering data from Refs. 4,5,38,40.

any arbitrary **q** point (i.e., even a point not contained in the original grid). Because of the polar character of the group III nitrides, the dynamical matrix $D(\mathbf{q})$ displays nonanalytic behavior in the limit $\mathbf{q}\rightarrow 0$. It arises from the long-range character of the Coulomb force and has the well-known general form:

$$D^{\mathrm{na}}_{ss',\alpha\beta}(\mathbf{q}\rightarrow 0)\sim \frac{(\mathbf{q}\cdot\mathbf{Z}^{*}_{s})_{\alpha}(\mathbf{q}\cdot\mathbf{Z}^{*}_{s'})_{\beta}}{\mathbf{q}\cdot\epsilon^{\infty}\cdot\mathbf{q}},$$

TABLE III. Zone-center phonon frequencies for wurtzite AlN, GaN, and InN in units of cm^{-1}.

		E_2^l	B_1^l	A_1(TO)	E_1(TO)	E_2^h	B_1^h	A_1(LO)	E_1(LO)
AlN	This work	233	547	614	666	655	719	875	898
	Theory [a]			619	677			893	918
	Theory [b]	236	553	629	649	631	717		
	Theory [c]			610	710				
	Theory [d]	247	636	612	679	672	645		
	Experiment [e]	252		614	673	660		893	916
	Experiment [f]	241		607		660			924
GaN	This work	138	334	550	572	574	690	733	737
	Theory [g]	143	337	541	568	579	720	748	757
	Theory [b]	150	330	537	555	558	677		
	Theory [c]			570	585				
	Theory [d]	185	526	544	566	557	584		
	Experiment [h]	145		533	561	570		735	742
InN	This work	83	225	443	467	483	576	586	595
	Experiment [i]					495		596	
	Experiment [j]					491		590	

[a]DFPT, pseudopotential, Karch *et al.* Ref. 7.
[b]Frozen phonon, full potential linear muffin-tin orbital (FP-LMTO), Gorczyca *et al.* Ref. 36.
[c]Frozen phonon, FP-LMTO, Kim *et al.* Ref. 37.
[d]Frozen phonon, pseudopotential, Shimada *et al.* Ref. 28.
[e]Raman data, McNeil *et al.* Ref. 38.
[f]Raman data, Perlin *et al.* Ref. 39.
[g]DFPT, pseudopotential, Karch *et al.* Ref. 6.
[h]Raman data, Filippidis *et al.* Ref. 40.
[i]Raman data, Kwon *et al.* Ref. 4.
[j]Raman data, Lee *et al.* Ref. 5.

where ϵ^{∞} is the high-frequency dielectric tensor and $\mathbf{Z}_s^*$ is the Born effective-charge tensor for the atom s. This nonanalyticity in reciprocal space would correspond to very long-range interatomic force constants in real space, which are difficult to treat. Therefore, a term that contains the above-mentioned nonanalyticity is subtracted from the dynamical matrices at each q point in the grid. Fourier analysis of these modified dynamical matrices provides the short-range contribution to the interatomic force constants. These short-range interatomic force constants and the nonanalytic term can then be used to compute the dynamical matrices at any arbitrary $\mathbf{q}$ point. Following Ref. 9, we used the nonanalytic term obtained from the Coulomb interaction of pointlike ions, generalized to take into account the anisotropy of the wurtzite structure. For a proper treatment of this term, only the Born effective charges and the high-frequency dielectric tensor are needed, both of which can be calculated within the DFPT. We found that the grid $(LMN)=(664)$, with $\mathbf{G}_3$ parallel to the c axis of wurtzite, provides a good description of the short-range contribution to the interatomic force constants.

III. RESULTS AND DISCUSSION

The values of the calculated structural parameters are reported in Table I. They are in good agreement with the experimental values and with the results of other calculations. For GaN, the structural parameters obtained with the NLCC give the same degree of accuracy as those obtained with the d electrons in valence, in agreement with previous investigations.[7,15] For InN, the NLCC overestimates the bulk modulus, and a pseudopotential with the $4d$ electrons in the valence is needed to have a more accurate description. We attribute the major role played by the d electrons in InN to the fact that the $4d$ semicore electrons of In extend further outside the core and have a larger overlap with the valence states than the $3d$ electrons of Ga. Furthermore, the $4d$ electrons in the In atom are more resonant with the $2s$ electrons of N than the $3d$ in the Ga atom.

To deal with the macroscopic electric field associated with the longitudinal optical modes and the related nonanalytic behavior of the dynamical matrix at Γ, we have calculated the dielectric tensors and the Born effective-charge tensors for AlN, GaN, and InN. The components of ϵ^{∞} and $\mathbf{Z}^*$ perpendicular ($\perp$) and parallel ($\parallel$) to the c axis are reported in Table II together with their average values. The agreement with the experimental data, which are scarce, and from samples with many defects, and with the other theoretical values is good. Our values for the dielectric tensors in GaN and AlN are about 8% larger than the experimental ones, as expected on the basis of previous calculations for III-V,[19] II-VI,[20] and group IV (Ref. 9) semiconductors; it is well known that the LDA approximation tends to overestimate the electronic screening.[21] We notice that the Born charges for

the III-nitrides follow the same trend as the static ionicities, as measured by the charge asymmetry coefficients[22] $g_{\mathrm{AlN}}=0.79$, $g_{\mathrm{GaN}}=0.78$, and $g_{\mathrm{InN}}=0.85$, indicating that InN has larger dynamical and static ionicities than AlN and GaN (which are similar). The screened effective charge $\mathbf{Z}^*/\sqrt{\epsilon^{\infty}}$ does not follow the same trend as the static ionicity, but increases in going from InN to AlN. This is because $\mathbf{Z}^*$ is similar in GaN and AlN but larger in InN, while ϵ^{∞} increases going from AlN to InN.

In Fig. 1, the calculated phonon-dispersion curves of AlN, GaN, and InN in the wurtzite structure are shown along several high symmetry lines in the BZ, together with the corresponding one-phonon density of states (DOS). The frequency scales for AlN, GaN, and InN are mainly determined by the masses of the cation species, Al, Ga, and In. Since the unit cell contains four atoms, there are 12 vibrational normal modes producing a complicated ''spaghettilike'' dispersion. The situation is simplified along those directions where the irreducible representations have higher dimensions. For example, along the direction ΓA (Δ line) there are only eight modes: four longitudinal modes belonging to the one-dimensional representations Δ_1 and Δ_4, and four transverse modes belonging to the two-dimensional representations $\Delta_5^{(2)}$ and $\Delta_6^{(2)}$ ($\Delta=2\Delta_1+2\Delta_4+2\Delta_5^{(2)}+2\Delta_6^{(2)}$). At the point A there are only four modes: two doubly degenerate longitudinal modes, and two fourfold degenerate transverse modes. The acoustic-phonon branches are well separated from the optical ones in all of the three materials, but the gap between the branches, clearly seen in the DOS, is larger in InN and smaller in AlN, due to the different mass mismatches between the cations and the nitrogen. Another difference in the phonon spectra is that the LO mode (the highest frequency branch) in AlN is more dispersive than in GaN and InN. This is due to the larger LO-TO splitting of AlN. Defining the relative splitting as $(\omega_{\mathrm{LO}}-\omega_{\mathrm{TO}})/\omega_{\mathrm{TO}}$, we have for the E_1 (A_1) mode: 0.35 (0.43) in AlN, 0.29 (0.33) in GaN, and 0.27 (0.32) in InN. As can been seen in Fig. 1, in the wurtzite nitrides there is no gap between the LO and TO phonon branches whereas a gap is present in zb-GaN and zb-AlN.[6,7]

The lifetime of LO phonons can determine the hot-phonon effects[23] which, for the case of GaAs, are known to play a central role in the relaxation of hot carriers on very short time scales, and therefore, in device performance. However, the decay processes of the LO phonons in the III-nitrides are still poorly characterized. Our calculated phonon dispersions indicate that the three phonon process, namely the decay of a zone-center LO phonon into two LA or TA phonons of equal frequencies and opposite wave vectors, is not possible in GaN and InN because $\omega_{\mathrm{LO}}>2\omega_{\mathrm{LA,TA}}$ over the whole spectrum. This three-phonon process is usually an allowed decay channel of LO phonons in other III-V semiconductors. In agreement with our results, time-resolved Raman studies suggest that LO phonons in GaN decay primarily into a large wave-vector TO and a large wave-vector LA or TA phonon, and not into two acoustic phonons.[24]

A comparison with experiment is possible only at the zone center. For the Γ point (group symmetry C_{6v}), group theory predicts eight modes: $2A_1+2B_1+2E_1^{(2)}+2E_2^{(2)}$, of which one A_1 and one $E_1^{(2)}$ are both Raman active and infrared active; the two $E_2^{(2)}$ are only Raman active; and the B_1 modes are silent. Due to the macroscopic electric field associated with the atomic displacements of the longitudinal optical phonons, the A_1 and $E_1^{(2)}$ optical modes are each split into LO and TO components. In particular, as a result of the anisotropic nature of the wurtzite structure, these modes have an angular dependence. In Fig. 2 we show the angular dispersion of the optical modes at the Γ point; the angle θ is the angle between the c axis and the wave vector $\mathbf{q}\rightarrow 0$. Taking the angular dispersion of the TO modes, $[\omega_{\mathrm{TO}}(E_1)-\omega_{\mathrm{TO}}(A_1)]/\omega_{\mathrm{TO}}(E_1)$ as a measure of the crystal anisotropy, we find 0.08 for AlN, 0.04 for GaN, and 0.05 for InN. AlN is thus more anisotropic than GaN and InN.

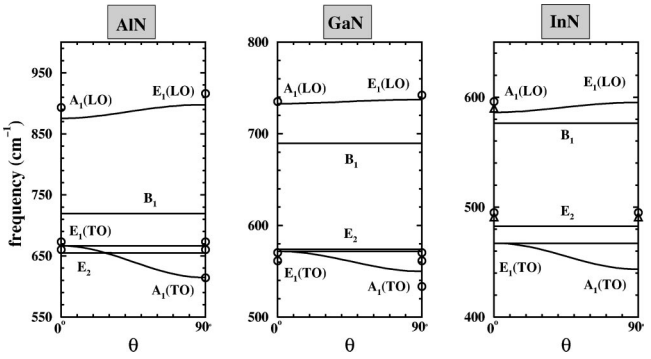

FIG. 2. Angular dispersion of the optical-phonon modes in wurtzite AlN, GaN, and InN at Γ. The angle θ is the angle between the c axis and the wave vector $\mathbf{q}\rightarrow 0$. Experimental data are taken from Refs. 4,5,38,40.

The values of the phonon frequencies at Γ are given in Table III. The overall agreement between our results and the experimental data is good and within the typical accuracy of DFPT calculations, namely 1–3%. For AlN and GaN, our results agree with previous calculations to within a few percent. InN is the least studied of the three nitrides; to the best of our knowledge there are no other phonon calculations and only a few recent Raman measurements.[4,5]

IV. SUMMARY

We have performed *ab initio* calculations of structural, dielectric and lattice-dynamical properties for AlN, GaN, and InN in the wurtzite structure. For GaN and AlN, we find good agreement with previous calculations and the available experimental zone-center data. For the phonons of InN, these are the first theoretical results. They agree well with the recent Raman data. The present calculations provide reliable predictions of the full phonon dispersions of AlN, GaN, and InN and have allowed us to compare the properties of these three materials. The relative magnitudes of the phonon frequencies in these materials are predominantly determined by the cation masses. Further, the relative mismatch between the cation and nitrogen masses leads to a broadening of the gap between the optical and the acoustic branches as one goes from AlN to InN. The dispersion of the LO mode displays the opposite behavior and decreases from AlN to InN, which reflects the narrowing of the LO-TO splitting as one proceeds down the column from Al to In. Finally, contrary to most III-V semiconductors, including AlN, the three-phonon decay channel of the LO phonon into two LA (TA) phonons of same energy is not allowed in GaN and InN due to the fact

that $\omega_{LO} > 2\omega_{LA(TA)}$ over the whole spectrum. This could affect the lifetime of the LO phonons and consequently determine the hot-phonon related effects, which play an important role in the transport properties of hot carriers and in the performance of high-speed devices.

ACKNOWLEDGMENTS

This work was supported in part by ONR and NSF. The calculations were carried out at the North Carolina Supercomputing Center.

*Electronic address: bungaro@sissa.it

[1] T. D. Moustakas, T. Lei, and R. J. Molnar, Physica B **185**, 36 (1992); H. Okumura, K. Ohta, G. Feuillet, K. Balakrishnan, S. Chichibu, H. Hamaguchi, P. Hacke, and S. Yoshida, J. Cryst. Growth **178**, 113 (1997).
[2] J.C. Nipko and C.K. Loong, Phys. Rev. B **57**, 10 550 (1998).
[3] J.C. Nipko, C.K. Loong, C.M. Balkas, and R.F. Davis, Appl. Phys. Lett. **73**, 34 (1998).
[4] H.J. Kwon, Y.H. Lee, O. Miki, H. Yamano, and A. Yoshida, Appl. Phys. Lett. **69**, 937 (1996).
[5] M.C. Lee, H.C. Lin, Y.C. Pan, C.K. Shu, J. Ou, W.H. Chen, and W.K. Chen, Appl. Phys. Lett. **73**, 2606 (1998).
[6] K. Karch, J. M. Wagner, and F. Bechstedt, Phys. Rev. B **57**, 7043 (1998).
[7] K. Karch and F. Bechstedt, Phys. Rev. B **56**, 7404 (1997).
[8] S. Baroni, P. Giannozzi, and A. Testa, Phys. Rev. Lett. **58**, 1861 (1987).
[9] P. Giannozzi, S. de Gironcoli, P. Pavone, and S. Baroni, Phys. Rev. B **43**, 7231 (1991).
[10] G.B. Bachelet, D.R. Hamann, and M. Schlüter, Phys. Rev. B **26**, 4199 (1982).
[11] D.R. Hamann, M. Schlüter, and C. Chiang, Phys. Rev. Lett. **43**, 1494 (1979).
[12] D.R. Hamann, Phys. Rev. B **40**, 2980 (1989).
[13] L. Kleinman and D.M. Bylander, Phys. Rev. Lett. **48**, 1425 (1982).
[14] K. Rapcewicz, M. Buongiorno Nardelli, and J. Bernholc, Phys. Rev. B **56**, R12 725 (1997).
[15] M. Buongiorno Nardelli, K. Rapcewicz, and J. Bernholc, Phys. Rev. B **55**, R7323 (1997).
[16] K. Karch, F. Bechstedt, and T. Pletl, Phys. Rev. B **56**, 3560 (1997).
[17] N. Troullier and J.L. Martins, Phys. Rev. B **43**, 1993 (1991).
[18] D.J. Chadi and M.L. Cohen, Phys. Rev. B **8**, 5747 (1973).
[19] P. Pavone, K. Karch, O. Schütt, W. Windl, D. Strauch, P. Giannozzi, and S. Baroni, Phys. Rev. B **48**, 3156 (1993).
[20] A. Dal Corso, S. Baroni, and R. Resta, Phys. Rev. B **47**, 3588 (1993).
[21] S. de Gironcoli, S. Baroni, and R. Resta, Phys. Rev. Lett. **62**, 2853 (1989).
[22] A. García and M.L. Cohen, Phys. Rev. B **47**, 4215 (1993).
[23] See, for example, *Proceedings of the 7th International Conference on Hot Carriers in Semiconductors*, edited by C. Hamaguchi and M. Inoue (Hilger, New York, 1992).
[24] K.T. Tsen, D.K. Ferry, A. Botchkarev, B. Sverdlov, A. Salvador, and H. Morkoc, Appl. Phys. Lett. **72**, 2132 (1998).
[25] A. Wright and J. Nelson, Phys. Rev. B **50**, 2159 (1994); **51**, 7866 (1995).
[26] N.E. Christensen and I. Gorczyca, Phys. Rev. B **50**, 4397 (1994).
[27] J. Chen, Z. Levine, and J.W. Wilkins, Appl. Phys. Lett. **66**, 1129 (1994).
[28] K. Shimada, T. Sota, and K. Suzuki, J. Appl. Phys. **84**, 4951 (1998).
[29] F. Bernardini, V. Fiorentini, and D. Vanderbilt, Phys. Rev. B **56**, R10 024 (1997).
[30] J.A. Sanjurjo, E. López-Cruz, P. Vogl, and M. Cardona, Phys. Rev. B **28**, 4579 (1983).
[31] A.T. Collins, E.C. Leitowlers, and P.J. Dean, Phys. Rev. **158**, 833 (1967).
[32] L. Akasaki and M. Hashimoto, Solid State Commun. **5**, 851 (1967).
[33] A. S. Barker and M. Ilegems, Phys. Rev. B **7**, 743 (1973).
[34] D. D. Manchon, A. S. Barker, P. J. Dean, and R. B. Zetterstrom, Solid State Commun. **8**, 1227 (1970).
[35] J. Misek and F. Srobar, Elektrotech. Cas. **30**, 690 (1979).
[36] I. Gorczyca, N.E. Christensen, E.L. Pelzer y Blancá, and C.O. Rodriguez, Phys. Rev. B **51**, 11 936 (1995).
[37] K. Kim, W. R. L. Lambrecht, and B. Segall, Phys. Rev. B **53**, 16 310 (1996).
[38] L.E. McNeil, M. Grimsditch, and R.H. French, J. Am. Ceram. Soc. **76**, 1132 (1993).
[39] P. Perlin, A. Polian, and T. Suski, Phys. Rev. B **47**, 2874 (1993).
[40] L. Filippidis, H. Siegle, A. Hoffmann, C. Thomsen, K. Karch, and F. Bechstedt, Phys. Status Solidi B **198**, 621 (1996).